Research Article | Vol. 24, No. 20 | 3 Oct 2016 | OPTICS EXPRESS 22796

Optics EXPRESS

Exploring vortex structures in orbital-angular-momentum beams generated from planar geometric modes with a mode converter

J. C. TUNG,[1] H. C. LIANG,[2] T. H. LU,[3] K. F. HUANG,[1] AND Y. F. CHEN[1,*]

[1]*Department of Electrophysics, National Chiao Tung University, 1001, Ta-Hsueh Rd., Hsinchu 30010, Taiwan*
[2]*Institute of Optoelectronic Science, National Taiwan Ocean University, 2 Pei-Ning Rd., Keelung 20224, Taiwan*
[3]*Department of Physics, National Taiwan Normal University, 88 Ting-Chou Rd., Sec. 4, Taipei 11677, Taiwan*
[*]*yfchen@cc.nctu.edu.tw*

Abstract: It is theoretically demonstrated that the planar geometric mode with a π/2 mode converter, so called the circularly geometric mode, can be solved from the inhomogeneous Helmholtz equation by considering the pump distribution on the lasing mode. Theoretical analysis clearly reveal that the vortex structures of circularly geometric modes are determined by the minimum order of transverse lasing modes, the total number of transverse lasing modes and the degenerate condition in the cavity. Moreover, we experimentally manifest that the circularly geometric mode can be generated from the selective pumped solid-state laser with an external π/2 mode converter. To explore the vortex structures of the generated geometric modes, the interference patterns are performed by an experimental apparatus consisting of a Mach-Zehnder interferometer. The good agreement between experimental observations and numerical calculations confirms the analysis of vortex structures is reliable.

OCIS codes: (050.4865) Optical vortices; (140.3295) Laser beam characterization; (140.3580) Lasers, solid-state.

References and links

1. K. T. Gahagan and G. A. Swartzlander, Jr., "Optical vortex trapping of particles," Opt. Lett. **21**(11), 827–829 (1996).
2. M. Dienerowitz, M. Mazilu, P. J. Reece, T. F. Krauss, and K. Dholakia, "Optical vortex trap for resonant confinement of metal nanoparticles," Opt. Express **16**(7), 4991–4999 (2008).
3. M. P. MacDonald, G. C. Spalding, and K. Dholakia, "Microfluidic sorting in an optical lattice," Nature **426**(6965), 421–424 (2003).
4. K. Toyoda, K. Miyamoto, N. Aoki, R. Morita, and T. Omatsu, "Using optical vortex to control the chirality of twisted metal nanostructures," Nano Lett. **12**(7), 3645–3649 (2012).
5. K. Toyoda, F. Takahashi, S. Takizawa, Y. Tokizane, K. Miyamoto, R. Morita, and T. Omatsu, "Transfer of light helicity to nanostructures," Phys. Rev. Lett. **110**(14), 143603 (2013).
6. G. Molina-Terriza, J. P. Torres, and L. Torner, "Twisted photons," Nat. Phys. **3**(5), 305–310 (2007).
7. G. Gibson, J. Courtial, M. Padgett, M. Vasnetsov, V. Pas'ko, S. Barnett, and S. Franke-Arnold, "Free-space information transfer using light beams carrying orbital angular momentum," Opt. Express **12**(22), 5448–5456 (2004).
8. A. Jesacher, S. Fürhapter, S. Bernet, and M. Ritsch-Marte, "Spiral interferogram analysis," J. Opt. Soc. Am. A **23**(6), 1400–1409 (2006).
9. Y. F. Chen, Y. P. Lan, and S. C. Wang, "Generation of Laguerre–Gaussian modes in fiber-coupled laser diode end-pumped lasers," Appl. Phys. B **72**(2), 167–170 (2001).
10. E. Abramochkin and V. Volostnikov, "Beam transformations and nontransformed beams," Opt. Commun. **83**(1–2), 123–135 (1991).
11. L. Allen, M. W. Beijersbergen, R. J. C. Spreeuw, and J. P. Woerdman, "Orbital angular momentum of light and the transformation of Laguerre-Gaussian laser modes," Phys. Rev. A **45**(11), 8185–8189 (1992).
12. M. W. Beijersbergen, L. Allen, H. E. L. O. van der Veen, and J. P. Woerdman, "Astigmatic laser mode converters and transfer of orbital angular momentum," Opt. Commun. **96**(1–3), 123–132 (1993).
13. M. W. Beijersbergen, R. P. C. Coerwinkel, M. Kristensen, and J. P. Woerdman, "Helical-wavefront laser beams produced with a spiral phaseplate," Opt. Commun. **112**(5–6), 321–327 (1994).

#273296 http://dx.doi.org/10.1364/OE.24.022796
Journal © 2016 Received 8 Aug 2016; revised 14 Sep 2016; accepted 17 Sep 2016; published 21 Sep 2016

Optics EXPRESS

14. V. Yu. Bazhenov, M. S. Soskin, and M. V. Vasnetsov, "Screw dislocations in light wavefronts," J. Mod. Opt. **39**(5), 985–990 (1992).
15. Y. J. Liu, X. W. Sun, D. Luo, and Z. Raszewski, "Generating electrically tunable optical vortices by a liquid crystal cell with patterned electrode," Appl. Phys. Lett. **92**(10), 101114 (2008).
16. Ya. Izdebskaya, V. Shvedov, and A. Volyar, "Generation of higher-order optical vortices by a dielectric wedge," Opt. Lett. **30**(18), 2472–2474 (2005).
17. A. B. Matsko, A. A. Savchenkov, D. Strekalov, and L. Maleki, "Whispering gallery resonators for studying orbital angular momentum of a photon," Phys. Rev. Lett. **95**(14), 143904 (2005).
18. J. Erhard, H. Laabs, B. Ozygus, and H. Weber, "Diode-pumped multipath laser oscillators," in Laser Resonators II, A. V. Kudryashov, ed., Proc. SPIE **3611**, 2–10 (1999)
19. Q. Zhang, B. Ozygus, and H. Weber, "Degeneration effects in laser cavities," Eur. Phys. J. Appl. Phys. **6**(3), 293–298 (1999).
20. J. Dingjan, M. P. van Exter, and J. P. Woerdman, "Geometric modes in a single-frequency Nd: YVO_4 laser," Opt. Commun. **188**(5–6), 345–351 (2001).
21. Y. F. Chen, C. H. Jiang, Y. P. Lan, and K. F. Huang, "Wave representation of geometrical laser beam trajectories in a hemiconfocal cavity," Phys. Rev. A **69**(5), 053807 (2004).
22. A. A. Malyutin, "Modes of a plano-spherical laser resonator with the Gaussian gain distribution of the active medium," Quantum Electron. **37**(3), 299–306 (2007).
23. A. A. Malyutin, "Closed laser-beam trajectories in plano-spherical resonators with Gaussian apertures," Quantum Electron. **38**(2), 181–186 (2008).
24. C. H. Chen, P. Y. Huang, and C. W. Kuo, "Geometric modes outside the multi-bouncing fundamental Gaussian beam model," J. Opt. **12**(1), 015708 (2010).
25. T. H. Lu, Y. C. Lin, Y. F. Chen, and K. F. Huang, "Generation of multi-axis Laguerre–Gaussian beams from geometric modes of a hemiconfocal cavity," Appl. Phys. B **103**(4), 991–999 (2011).
26. Y. F. Chen, J. C. Tung, P. Y. Chiang, H. C. Liang, and K. F. Huang, "Exploring the effect of fractional degeneracy and the emergence of ray-wave duality in solid-state lasers with off-axis pumping," Phys. Rev. A **88**(1), 013827 (2013).

1. Introduction

Over the past decades, the orbital angular momentum (OAM) or optical vortice has been exploited in a variety of applications, such as trapping [1,2] and rotating [3] of microscopic particles in hydrodynamics and biology, controlling the chirality of twisted metal nanostructures [4,5], quantum communication [6,7], and spiral interferometry [8]. Thus far the OAM can be generated from several special cases of laser modes with different techniques, such as generation of Laguerre-Gaussian (LG) modes [9], transformation from Hermite-Gaussian (HG) modes by lens coverters [10–12], and creation with Gaussian beams through spiral phase plates [13], synthesized holograms [14], spatial light modulation on liquid crystal cells [15] or dielectric wedges [16]. Nowadays, generation of light beams with huge OAM is an important and interesting task for potential applications including demonstration of optomechanical effects and trapping of cold atoms [17]. Therefore, the investigation of high-order laser modes is useful for developing the idea for generating the coherent structured light that can carry huge OAM.

Selective pumping is an interesting method to yield high-order transverse modes. Recently, the Herriott-type multipass beams, known as planar geometric modes, have been experimentally found under the selective pumping [18–24]. The lasing modes have a preference to be localized on the periodic ray trajectories when the cavity lengths are somewhat close to the degenerate cavities. More intriguingly, the planar geometric modes formed by the coherent superposition of HG eigenmodes could be converted into the corresponding LG modes by a $\pi/2$-cylindrical-lens mode converter for producing huge OAM. Although it has been verified that the planar geometric modes can be transformed into the circularly geometric modes by using a mode converter [25], there has been no study with regard to the vortex structures related to the circularly geometric modes thus far.

In this work we exploit the inhomogeneous Helmholtz equation to manifest a theoretical analysis of the circularly geometric modes performed by using the eigenmode expansion for considering the pump distribution on the lasing mode in Ref [26]. Through numerical calculations of the phase distribution, it can be found that the topological charge of the central singularity is determined by the minimum order of transverse lasing eigenmodes. Moreover,

Optics EXPRESS

the number of singularities and the vortex distributions surrounding outside are decided by not only the minimum order of transverse lasing eigenmodes, but also the total number of transverse lasing eigenmodes and the degenerate condition in the cavity. In experiments, we use the selective pumped microchip laser with an external π/2-cylindrical-lens mode converter to generate the circularly geometric modes. To analyze vortex structures of generated geometric modes, the experimental equipment with a Mach-Zehnder interferometer is also employed to display the desired interference patterns. Note that the interference pattern is formed by the plane wave and the circularly geometric mode. It is found that the experimental interference pattern can be excellently reconstructed with the theoretical model. Furthermore, the experimental interference patterns formed by a tilted plane wave and a circularly geometric mode can agree very well with the numerical calculations. The good agreement confirms that an analysis of vortex structures for circularly geometric modes in the present theoretical model is trustworthy.

2. Theoretical analysis of vortex structures generated by a π/2 mode converter

Under the paraxial approximation, the eigenmodes for the laser cavity with a concave mirror at $z = -L$ and a plane mirror at $z = 0$ can be expressed as the $HG_{n,m}$ modes, where n and m are the transverse indices in x- and y- directions. Considering $m = 0$, the eigenmodes are given by:

$$\psi_{n,s}(x,y,z) = \Phi_n(x,y,z)\exp\left(-ik_{n,s}\tilde{z}\right)\exp\left[i(n+1)\theta_G(z)\right], \tag{1}$$

where

$$\Phi_n(x,y,z) = \sqrt{\frac{2}{2^n \pi\, n!}}\frac{1}{w(z)}H_n\left(\frac{\sqrt{2}\,x}{w(z)}\right)\exp\left[-\frac{x^2+y^2}{w(z)^2}\right], \tag{2}$$

s is the longitudinal index, H_n (•) is the Hermite polynomial of order n, $k_{n,s} = 2\pi f_{n,s}/c$, $f_{n,s}$ is the eigenmode frequency, $z_R = \sqrt{L(R-L)}$ is the Raleigh range, R is the radius of curvature of the concave mirror, $\theta_G(z) = \tan^{-1}\left(z/z_R\right)$ is the Gouy phase, $w(z) = w_o\sqrt{1+(z/z_R)^2}$, $w_o = \sqrt{\lambda z_R/\pi}$ is the beam radius at the waist, $\tilde{z} = z + [(x^2+y^2)z]/[2(z^2+z_R^2)]$, and λ is the emission wavelength. With the transformation of spatial morphologies, the corresponding $LG_{p,\ell}$ modes for the radial index p and the azimuthal index ℓ can be expressed as:

$$\tilde{\psi}_{n,s}^{(\pm)}(\rho,\phi,z) = \tilde{\Phi}_n^{(\pm)}(\rho,\phi,z)\exp\left(-ik_{n,s}\tilde{z}\right)\exp\left[i(n+1)\theta_G(z)\right], \tag{3}$$

with

$$\tilde{\Phi}_n^{(\pm)}(\rho,\phi,z) = \sqrt{\frac{2}{\pi\, n!}}\frac{1}{w(z)}\left(\frac{\sqrt{2}\rho}{w(z)}\right)^n\exp\left[-\frac{\rho^2}{w(z)^2}\right]\exp\left(\pm i n\phi\right). \tag{4}$$

Note that $\tilde{\psi}_{n,s}^{(\pm)}(\rho,\phi,z)$ in Eq. (3) is explicitly the azimuthal-order $LG_{0,n}$ eigenmodes. With planar geometric modes expressed as the expansion of HG eigenmodes satisfying the inhomogeneous Helmholtz equation [26], it is intriguing to explore the spatial morphology of planar geometric modes by transforming each HG components into the corresponding LG modes. Under the selective pumping, the transformed modes, also called circularly geometric modes, can be expressed as:

Optics EXPRESS

$$\Psi^{(\pm)}(\rho,\phi,z)=\frac{\eta\,\lambda\,L'}{4\pi^2\,L_c}\sqrt{\frac{2}{\pi\,w^2(z_c)}}\,\frac{1}{\sqrt{\sqrt{2\pi\,n_o}}}\times\left\{\sum_{s=s_o-J}^{s_o+J}\sum_{n=n_o-N}^{n_o+N}\frac{\exp[-(n-n_o)^2/4n_o]}{[(s_o-s)+(n_o-n)\Omega]+i\gamma}\tilde{\psi}_{n,s}^{(\pm)}(\rho,\phi,z)\right\},\tag{5}$$

where n_o is the central transverse order, s_o is the central longitudinal order, z_c is the location of the gain medium, γ represents the inverse quality factor, and η is a constant that includes the effective conversion efficiency and the overlap integral in the longitudinal direction. The eigenmode frequency of the concave-plano cavity can be given by $f_{n,s}=[s\cdot\Delta f_L+(n+1)\cdot\Delta f_T]$. The transverse mode spacing Δf_T is given by $\Delta f_T=\Delta f_L\cdot[(1/\pi)\tan^{-1}(L/z_R)]$, where $\Delta f_L=c/2L'$, $L'=L+[n_c-(1/n_c)]L_c$, n_c is the refractive index of the gain medium, L_c is the physical length of the gain medium, and the mode-spacing ratio is $\Omega=\Delta f_T/\Delta f_L$. To fulfill the degenerate condition, the mode-spacing ratio requires satisfying the fractional degeneracy of $\Omega=P/Q$, where P and Q are co-prime integers. $2N+1$ and $2J+1$ are the total number of the transverse and longitudinal eigenmodes, respectively; J is the integer closest to $N\Omega$. To clarify the $LG_{0,n}$ eigenmodes contributed in the circularly geometric modes, we set $\Delta f_L=Q\cdot f_o$ and $\Delta f_T=P\cdot f_o$, and f_o is the common factor of frequencies. The indices n and s are expressed as n_o+QK and s_o-PK for any integers K . Consequently, the eigenmode frequency can be normalized as $f_{n,s}/f_o=[s_o\cdot Q+(n_o+1)\cdot P]$. For the resonant condition, $k=k_{n,s}$ for $k=2\pi/\lambda$, the circularly geometric mode in Eq. (5) can be further expressed as a superposition of the degenerate eigenmodes:

$$\Psi^{(\pm)}(\rho,\phi,z)=\frac{\eta}{L_c}\sqrt{\frac{2}{\pi\,w^2(z_c)}}\,\frac{\exp(-ik\,\tilde{z})}{\sqrt{\sqrt{2\pi\,n_o}}}\times\left[\sum_{n=n_o+QK}e^{-\frac{(n-n_o)^2}{4n_o}}\tilde{\Phi}_n^{(\pm)}(\rho,\phi,z)\,e^{i(n+1)\theta_G(z)}\right],\tag{6}$$

where $-[N/Q]\le K\le[N/Q]$, and $[u]$ denotes the largest integer $\le u$. Equation (6) clearly indicates that the circularly geometric modes are formed by $\tilde{\Phi}_n^{(\pm)}(\rho,\phi,z)$ with various order n.

To further verify the vortex structures of circularly geometric modes, phase singularities are conventionally described in terms of the phase angle field $\Theta(\rho,\phi)=\tan^{-1}\left(\mathrm{Im}[\Psi^{(\pm)}(\rho,\phi,z)]\ /\mathrm{Re}[\Psi^{(\pm)}(\rho,\phi,z)]\right)$ for a constant z, where $\mathrm{Re}[\Psi^{(\pm)}(\rho,\phi,z)]$ and $\mathrm{Im}[\Psi^{(\pm)}(\rho,\phi,z)]$ are the real and imaginary parts of the field $\Psi^{(\pm)}(\rho,\phi,z)$. The vortices of $\Theta(\rho,\phi)$ are the singularities at which the phase angle of the field $\Psi^{(\pm)}(\rho,\phi,z)$ is undefined. For convenience, we take the parameter N to be the integral multiple of Q , i.e., $N=K\,Q$. From the theoretical analysis of the phase angle field $\Theta(\rho,\phi)$, it can be found that in addition to the central singularity at the origin with the topological charges of $n_{\min}=n_o-KQ$ determined by the minimum order of transverse lasing modes, there are $2KQ$ singularities surrounding on the $n_{\min}$ groups of branches outside. Due to the equally distributed property, Q singularities require to be uniformly arrayed on the $n_{\min}$ groups of branches as far as possible. With the total number of the transverse eigenmodes to be $2KQ+1$, the number of singularities for the each group of branches increases with the

Optics EXPRESS

multiple of $2K$. Consequently, the topological charges for each group of branches are the components of $\{2Ku, 2K(u+1)\}$ for $n_{\min} < Q$, where u is the quotient of $Q / n_{\min}$. On the other hand, the topological charges for each group of branches are $2K$ for $n_{\min} = Q$ and the components of $\{0, 2K\}$ for $n_{\min} > Q$.

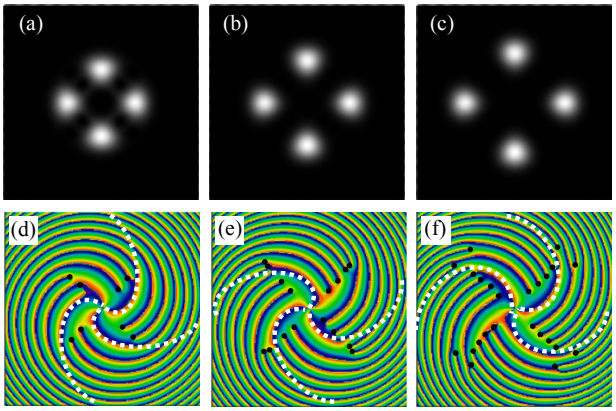

Fig. 1. (a)-(c) Calculated wave patterns $|\Psi^{(+)}(\rho,\phi,z)|^2$ for the case of $n_{min} < Q$ with $n_{min} = 3$, $Q = 4$, $n_o = 7$, 11 and 15 and $K = 1$, 2 and 3, respectively; (d)-(f) Numerical patterns of phase angle fields for $\Psi^{(+)}(\rho,\phi,z)$ corresponding to (a)-(c), respectively.

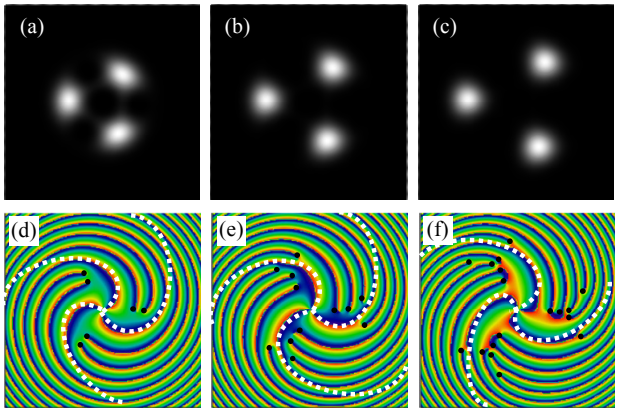

Fig. 2. (a)-(c) Calculated wave patterns $|\Psi^{(+)}(\rho,\phi,z)|^2$ for the case of $n_{min} = Q = 3$ with $n_o = 6$, 9 and 12 and $K = 1$, 2 and 3, respectively; (d)-(f) Numerical patterns of phase angle fields for $\Psi^{(+)}(\rho,\phi,z)$ corresponding to (a)-(c), respectively.

Optics EXPRESS

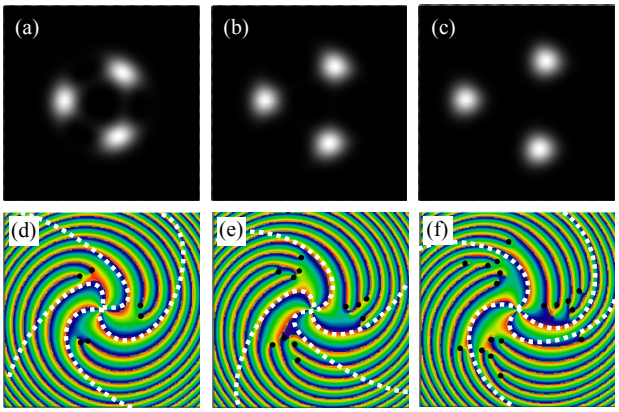

Fig. 3. (a)-(c) Calculated wave patterns $|\Psi^{(+)}(\rho,\phi,z)|^2$ for the case of $n_{min} > Q$ with $n_{min} = 4$, $Q = 3$, $n_o = 7$, 10 and 13 and $K = 1$, 2 and 3, respectively; (d)-(f) Numerical patterns of phase angle fields for $\Psi^{(+)}(\rho,\phi,z)$ corresponding to (a)-(c), respectively.

As seen in Figs. 1(a)-1(c), the circularly geometric modes $\left|\Psi^{(+)}(\rho,\phi,z)\right|^2$ at z = 10 mm are indicated with n_o = 7, 11 and 15, K = 1, 2 and 3, $Q = 4$ and the fixed central topological charge of $n_{\min} = 3$ for the case of $n_{\min} < Q$, respectively. The phase angle field $\Theta(\rho,\phi)$ depicted in Figs. 1(d)-1(f) exhibits that there are 8, 16 and 24 singularities represented by black dots surrounding outside, and the topological charges for each group of branches separated by white dotted curves are the components of {2, 4}, {4, 8} and {6, 12}, respectively. Figures 2(a)-2(c) reveal the circularly geometric modes with the parameters n_o = 6, 9 and 12, K = 1, 2 and 3 and $n_{\min} = Q = 3$. The number of singularities surrounding outside are 6, 12 and 18, and the topological charges for each group of branches are 2, 4 and 6 as shown in Figs. 2(d)-2(f), respectively. Furthermore, Figs. 3(a)-3(c) display the numerical results of the circularly geometric modes for the case of $n_{\min} > Q$ with the parameters n_o = 7, 10 and 13, K = 1, 2 and 3, $Q = 3$ and $n_{\min} = 4$, respectively. There are 6, 12 and 18 singularities surrounding outside, and the topological charges for each group of branches are the components of {0, 2}, {0, 4} and {0, 6} depicted in Figs. 3(d)-3(f). The promising manifestation not only accurately analyzes the vortex structures of circularly geometric modes but also provides a new attempt to employ the inhomogeneous Helmholtz equation to explore these structured beams.

3. Experimental results and discussions

To confirm the vortex structures of the circularly geometric modes in the experiment, we exploit the selective pumping to excite planar geometric modes in a concave-plano resonator as shown in Fig. 4. The laser medium is an *a*-cut 2.0-at.% Nd^{3+}:YVO_4 crystal with a length of 2 mm. Both sides of the Nd:YVO_4 crystal are coated for antireflection at 1064 nm (reflection < 0.1%). The radius of curvature of the concave mirror is R = 20 mm and the reflectivity is 99.8% at 1064 nm. The output coupler is a flat mirror with a transmission of 2% at 1064 nm. The pump source is an 809 nm fiber-coupled laser diode with a core diameter of 100 μm, a numerical aperture of 0.16, and a maximum output power of 3 W. A focusing lens with 20 mm focal length and 90% coupling efficiency is used to reimage the pump beam into the laser crystal. The pump radius is estimated to be approximately 25 μm. For a 20-mm radius-of-curvature concave mirror, it is found that the planar geometric mode could be realized when the optical cavity length L' is designed to be 18.5 mm. At a pump power of 1.5 W, the

Optics EXPRESS

emission power of the planar geometric mode with the off-axis displacement Δx = 0.3 mm can be seen to be 20 mW.

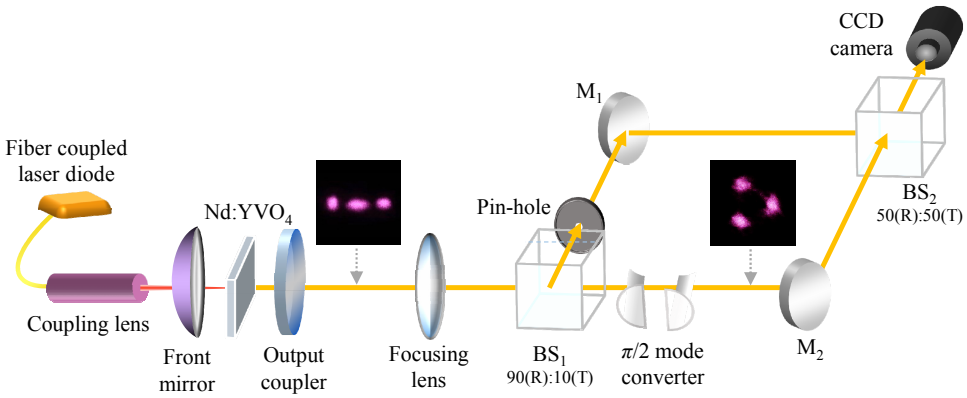

Fig. 4. Experimental setup for generating the interference patterns between plane waves and circularly geometric modes from a selective pumped solid-state lasers with an external π/2-cylindrical-lens mode converter.

For generating the interference patterns between plane waves and circularly geometric modes, the output planar geometric modes can be split into two beams after passing through a lens with focal length 125 mm and the beam splitter (BS_1). One sub-beam passes through a pin-hole with the radius 50 μm and the mirror M_1; the other sub-beam passes through a $\pi/2$ mode converter consisting of two cylindrical lenses and the mirror M_2. Note that the $\pi/2$-cylindrical-lens mode converter can transform the planar geometric modes into the circularly geometric modes when the axes of the cylindrical lenses are parallel to one another but at $\pm 45°$ to the principal axes of the planar geometric modes. The focal length of the cylindrical lenses is f = 25 mm; the distance is precisely adjusted to be $\sqrt{2}f$ for the operation of the $\pi/2$ converter. Interference patterns formed by recombining two sub-beams behind another beam splitter (BS_2) are imaged by a CCD camera.

Because of the circularly geometric modes formed by the superposition of the azimuthal-order $LG_{0,n}$ eigenmodes, the experimental interference patterns for $LG_{0,n}$ modes significantly shown in the first row of Fig. 5 manifest that the vortex structures of $LG_{0,n}$ modes could be flexibly generated from low to high orders under the present experimental approach. The second row of Fig. 5 depicts the contour plot of phase angle $\Theta(\rho,\phi)$ of the field $\tilde{\psi}_{n,s}^{(+)}(\rho,\phi,z)$ at z = 10 mm corresponding to the experimental results in the first row of Fig. 5. We can find that there is only a central singularity at the origin for each $LG_{0,n}$ mode with the topological charge of n. On the other hand, the numerical interference patterns between plane waves and the $LG_{0,n}$ modes can be further expressed as:

$$E(\rho,\phi,z) = \tilde{\psi}_{n,s}^{(+)}(\rho,\phi,z) + A\exp\left[i\left(k_z z + \vec{k}_t \cdot \vec{\rho}\right)\right], \tag{7}$$

where $k_z = k\cos\theta_z$, $\vec{k}_t = k\sin\theta_z\left(\cos\theta_t, \sin\theta_t\right)$ and A is the amplitude of plane waves. The calculated patterns $|E(\rho,\phi,z)|^2$ are shown in the third row of Fig. 5 for various azimuthal-order n with z = 10 mm and $\theta_z = \theta_t = 0$. It can be found that the numerical patterns agree very well with the experimental results in the first row of Fig. 5.

Optics EXPRESS

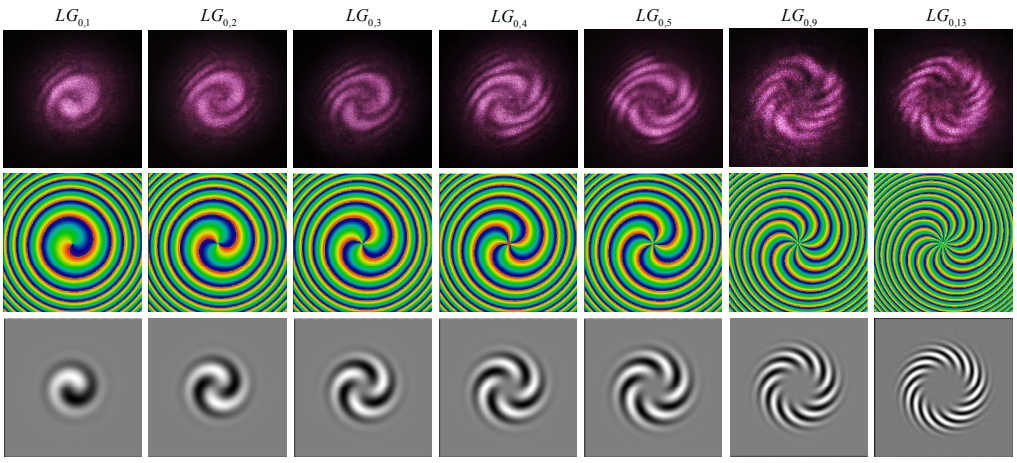

Fig. 5. (first row) Experimental interference patterns for $LG_{0,n}$ modes with various azimuthal-order n; (second row) Numerical patterns of phase angle fields for $LG_{0,n}$ modes; (third row) Calculated wave patterns corresponding to experimental results in the first row.

For investigating the experiment observations of circularly geometric modes under the selective pumping, the value of the parameter n_o signifies the magnitude of the off-axis displacement Δx with $n_o = [\Delta x / w(z_c)]^2$, and the effective range of mode index n can be limited as $|n - n_o| \le N$ with $N = 2\sqrt{n_o}$. For given values of the parameters $n_o = 13$, $N = 7$ $\Omega = 1/3$, z_c = 10 mm, z = 10 mm and λ = 1064 nm, the circularly geometric modes $\left|\Psi^{(+)}(\rho,\phi,z)\right|^2$ and $\left|\Psi^{(-)}(\rho,\phi,z)\right|^2$ calculated with Eq. (5) can be shown in Figs. 6(e) and 6(g), respectively. The theoretical patterns are in good agreement with the experimental results depicted in Fig. 6(a) and 6(c). To validate vortex structures of generated geometric modes, we also experimentally employ the plane wave to perform interference with the circularly geometric mode shown in Figs. 6(b) and 6(d). It can be seen that the inverse spiral directions for Figs. 6(b) and 6(d) are caused by rotating the axis of the mode converter with $\pm 45°$ to the principal axis of the planar geometric mode. Substituting $\Psi^{(\pm)}(\rho,\phi,z)$ into Eq. (7) to replace $\tilde{\psi}^{(+)}_{n,s}(\rho,\phi,z)$, the theoretical interference patterns are also depicted in Figs. 6(f) and 6(h) for comparison. From the phase angles $\Theta(\rho,\phi)$ for the fields $\Psi^{(\pm)}(\rho,\phi,z)$ in Figs. 6(e) and 6(g), the central topological charge of the circularly geometric modes is 7, the number of singularities surrounding outside is 12, and the topological charges for each group of branches are the components of {0, 4} for the parameters n_o = 13, K = 2 and $Q = 3$ satisfying the case of $n_{\min} > Q$. To the best of our knowledge this is the first exploration for vortex structures of the circularly geometric modes. We finally demonstrate the interference patterns for the circularly geometric mode by using a tilted plane wave. Figures 7 (b) and 7(c) depict the experimental results for the interference patterns between tilted plane waves and circularly geometric modes in Fig. 7(a). It can be seen that the experimental observations agree very well with the numerical patterns in Figs. 7(d)-(f). Here we use the parameters of $\theta_z = 6\times10^{-3}\pi$, $\theta_t = 0.2\pi$ in Fig. 7(e) and $\theta_z = 9\times10^{-3}\pi$, $\theta_t = 1.1\pi$ in Fig. 7(f). The good agreement confirms that the analysis of vortex structures in the present theoretical model is reliable.

Optics EXPRESS

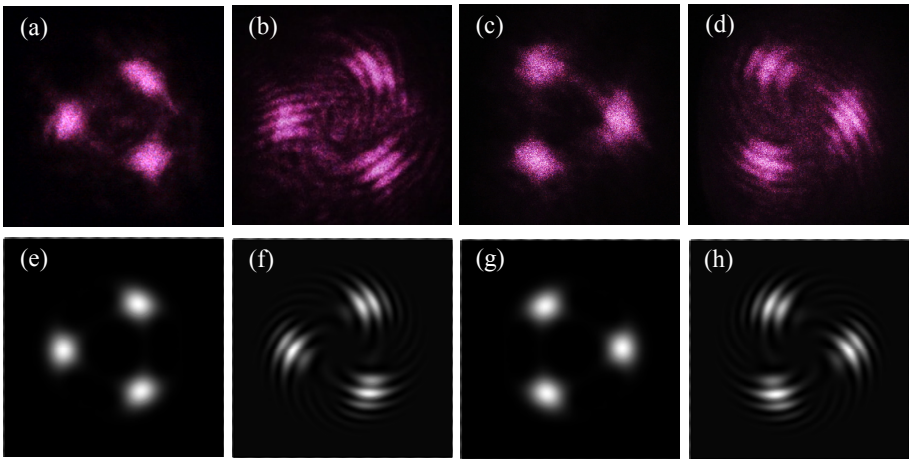

Fig. 6. (a) and (c) Experimental patterns of circularly geometric modes; (e) and (g) Calculated wave patterns $|\Psi^{(+)}(\rho,\phi,z)|^2$ and $|\Psi^{(-)}(\rho,\phi,z)|^2$ for $\Omega = 1/3$ corresponding to experimental results shown in (a) and (c), respectively; (b) and (d) Experimental interference patterns for circularly geometric modes; (f) and (h) Calculated wave patterns corresponding to experimental results in (b) and (d), respectively.

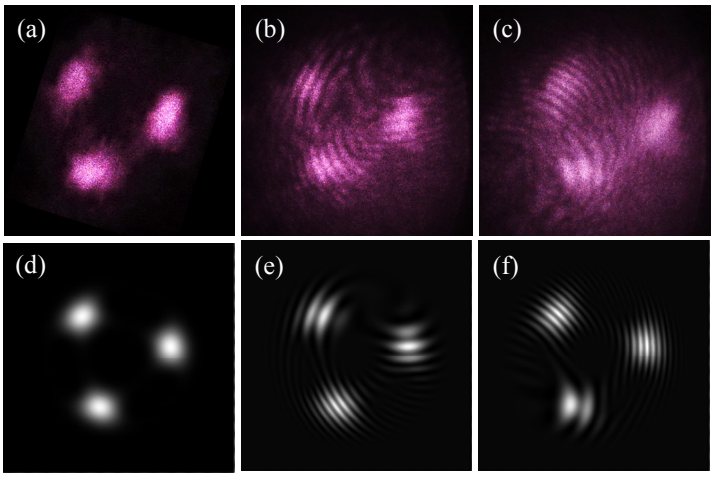

Fig. 7. (a) Experimental pattern of the circularly geometric mode; (b) and (c) Experimental interference patterns formed by tilted plane waves and circularly geometric modes; (d) Calculated wave patterns corresponding to experimental results in (a); (e) and (f) Calculated wave patterns with parameters $\theta_z = 6\times10^{-3}\pi$, $\theta_t = 0.2\pi$ and $\theta_z = 9\times10^{-3}\pi$, $\theta_t = 1.1\pi$ corresponding to experimental results in (b) and (c), respectively.

4. Conclusions

In summary, we employed a theoretical analysis of the eigenmode expansion satisfying the inhomogeneous Helmholtz equation to manifest the vortex structures of circularly geometric modes. It was theoretically indicated that in addition to the central singularity at the origin, there were several singularities surrounding outside. The topological charge of the central singularity was found to be determined by the minimum order of transverse lasing eigenmodes, and the number of outside singularities was controlled by the total number of transverse lasing eigenmodes and the degenerate condition in the cavity. Moreover, the topological charges for each group of branches were exhibited the significant dependence of the mode-spacing ratio in degenerate cavities and the minimum order of transverse lasing

Optics EXPRESS

eigenmodes. Furthermore, we employed the selective pumped solid-state laser with an external mode converter to generate the circularly geometric modes, and further exploited the Mach-Zehnder interferometer to display the interference pattern between the plane wave and the circularly geometric mode to investigate its vortex structures. It was clearly found that the numerical calculations agree very well with the experimental observations. Finally, we verified experimental and numerical interference patterns for circularly geometric modes by using a tilted plane wave to manifest the reliability of theoretical exploration. In addition to laser resonators with the selective pumping, spatial light modulators (SLMs) are the universal, adjustable, and widely applicable schemes for generating structured beams by controlling the phase of light distribution within an optical system. The intimate analysis of phase distribution in circularly geometric modes are also predictably applied to flexible SLMs. It is believed that the present exploration of circularly geometric modes can be used to develop in numerous optical manipulation because of their particular vortex structures and huge OAM.

Funding

This work is supported by the Ministry of Science and Technology of Taiwan (Contract No. MOST 105-2628-M-009-004).